The 8th European Congress on Computational Methods in Applied Sciences and Engineering
ECCOMAS Congress 2022
5-–9 June 2022, Oslo, Norway

INFLUENCE OF THE TURBULENT WAKE DOWNSTREAM OFFSHORE WIND TURBINES ON LARVAL DISPERSAL: DEVELOPMENT OF A NEW LAGRANGIAN-EULERIAN MODEL

Souha Ajmi[1], Martial Boutet[1], Anne-Claire Bennis[1*] & Jean-Claude Dauvin

[1] Normandy University, CNRS-UNICAEN-UNIROUEN, UMR 6143 M2C, 24 rue des Tilleuls, Caen, France.

[*] anne-claire.bennis@unicaen.fr

Key words: Environmental Fluid Mechanics, Marine Renewable Energy, Larval dispersal, Eulerian-Lagrangian coupling

Abstract. In the context of future offshore wind farms along the French coasts of the English Channel, the impacts of foundations on larval dispersal from bentho-pelagic species colonizing the hard substratum of artificial structures are studied in order to assess how the species connectivity could be modified by the farms. In particular, the effects of turbulent wake and horseshoe vortices are investigated. To this end, a new numerical approach is developed that combines the Eulerian model, OpenFoam, solving the 3D Navier-Stokes equations to compute the hydrodynamics, and the Lagrangian model, Ichthyop, based on an advection-diffusion equation to compute the larval trajectories. Firstly, some simple test cases are performed to validate the numerical coupling between OpenFoam and Ichthyop, such as the dispersion of larvae downstream a 2D cylinder in water. Secondly, the ability of OpenFoam turbulence models to simulate turbulent structures around monopile and gravity type foundations is evaluated. The RANS (Reynolds Averaged Navier-Stokes) k-omega SST turbulence model is chosen for the realistic application because it can reproduce the horseshoe vortices and turbulent wake with less computing time than the Smagorinsky LES (Large Eddy Simulation) model. Lastly, larval dispersal simulations for four benthic species and for a set of monopile and gravity foundations are performed. The main findings are: i) the larval material is transported onto the water column by 3D turbulence near the foundations and this transport for gravity foundation is modulated by the vertical geometry, with few larvae trapped behind the foundation, ii) the larval material follows the turbulent wake and few larvae are ejected outside the wake.

1 INTRODUCTION

Marine Renewable Energy is one of the most used in the European Union (EU) to contribute for a carbon free society. Offshore wind and tidal turbines, wave power, wind drones and others marine power represent a green energy source. By 2050, ocean energy can provide 450GW of electricity coming from offshore wind power. Besides, France has set ambitious targets of 40 GW by 2050 spread over 50 wind farms. For the moment, four Offshore Wind Farms (OWFs) are under construction off the French coast. Two of those OWFs are located in the Bay of Seine

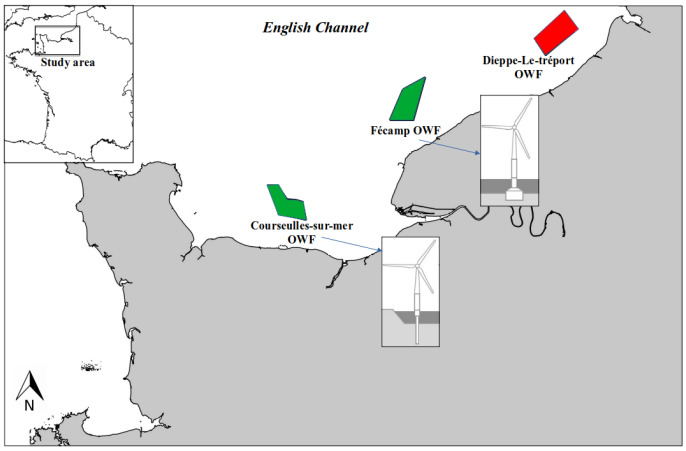

Figure 1: French offshore wind farms in the Bay of Seine area: two under construction [Courseulles-sur-Mer and Fécamp coasts (green areas)]; one under development phase [Dieppe-Le-Tréport coasts(red area)].

(see Figure 1). The Bay of Seine is known by its significant wind deposit, limited depth at 10 km from the coast and weather conditions which is favorable to development of offshore wind power. The area where the farms are located and the layout of the wind turbines within it constitutes an optimum making it possible to reconcile technical constraints (wind resource, depth, possibility of electrical connection) and constraints related to maritime safety, uses, the landscape and the environment. In this study, only the farms under construction (Courseulles-sur-Mer and Fécamp) are modelized because all the important data have been previously collected (e.g. bathymetry, geometry of the foundations). Courseulles-sur-Mer OWFs counts 64 turbines with 7MW each and Fécamp OWFS counts a total power approximetly equal to 500MW divided between 71 turbines. For [22] and [13], monopile structure is the most suited in Courseulles-sur-Mer OWFs site. This site has water depth variation between 20 and 30 m [20] and sandy-gravelly sea bottom (e.g. [20] and [19]). For Fécamp OWFs, as water depth varying between 30 to 39 m above mean sea level and seabed being flat and gravely, gravity base foundation is the technical and economical solution for the site. Coastal ocean structure like OWF foundations can affect ocean current at local scale, as shown in [2]; [4]; [20] and [21] for exemple. Scour protection systems deployed around turbine foundations can decrease current velocity downstream the structures favouring the particles deposition. The footprint of the foundation, in the presence of strong currents in the Bay of Seine, affects benthic and their pelagic phase especially during their planktonic life. As a result, it is necessary to study this effect [7]. Potential impacts of OWFs on benthic species were previously studied by [1]; [3]; [5]; [9]and [24]. To pursue former studies, simulations are set up here to modelize larval transport associated with the flow around monopile and gravity base structures.

This article is structured as follows: after an introduction, Section 2 describes the hydrodynamic model, the Lagrangian model and the coupling method. Section 3 presents the numerical results. Conclusions are dressed in Section 4.

2 METHODOLOGY

2.1 Eulerian model

Foundations of turbines represent an obstacle in the sea column for hydrodynamics. Interactions between flow and foundations depend on the structure and diameter of the turbine, but also the environmental forcing such as current flow. To evaluate the fluid-foundation interactions at local scale, CFD (Computational Fluid Dynamic) method was employed using OpenFOAM (Open Field Operation and Manipulation; [11]). This study focuses on local scale for each type of structure (monopile and gravity base). Modeling techniques in CFD simulate turbulence for incompressible flows using the Reynolds Averaged Navier-Stokes (RANS) method that involves to solve the continuity equation (1) and the momentum equation (2) as follows:

$$\nabla \cdot \vec{u} = 0, \tag{1}$$

$$\rho \frac{\partial \vec{u}}{\partial t} + (\vec{u} \cdot \vec{\nabla})\vec{u} = -\nabla p + \mu \nabla^2 \vec{u} + \vec{g}, \tag{2}$$

where $\vec{u}$ represents the flow velocity, p is the normalized pressure and $\vec{g}$ is acceleration of gravity. ρ and μ are the density and dynamic viscosity. The fluid flows with Reynolds number Re over 10^5 which can be calculated from the following equation:

$$Re = \frac{Ud}{\nu} \tag{3}$$

Where U is the undisturbed velocity, d is a diameter of the foundation (it could be monopile or gravity base foundation) and ν is kinematic viscosity. When the Reynolds number (Re) is between 3000 and 3.10^{+5}, the flow regime is turbulent. Hydrodynamics was simulated using the pimpleFOAM solver and the RANS k-omega SST (Shear Stress Transport) turbulence model [17] for its relevant computing time. This RANS model reproduces the turbulent flow by searching for the turbulent viscosity ν_t. k-omegaSST is a two equation model depending on time evolution equations for the turbulent kinetic energy (4) and turbulent dissipation (5) like it has used by [16]:

$$\frac{\partial \rho k}{\partial t} + \nabla(\rho u k) = \nabla(\Gamma_k \nabla k) + \widetilde{P_k} - D_k, \tag{4}$$

$$\frac{\partial \rho \omega}{\partial t} + \nabla(\rho u \omega) = \nabla(\Gamma_\omega \nabla \omega) + P_\omega - D_\omega + y_\omega, \tag{5}$$

with $\widetilde{P_k} = P_k - \beta \rho k \omega$ (where k, P_k, ω and β are the volumetric production rate of k, the turbulent kinetic energy, the turbulent dissipation rate and model constants, respectively). Γ_k and Γ_ω are the effective diffusivities for k and ω, and D_k and D_ω represent the turbulent dissipation terms. y_ω is the cross-diffusion term Eq.(5).

2.2 Boundary and initial conditions

The numerical model used is not suitable to compute the flow around foundation with the real scaling because of the high computational memory consuming. Therefore, a Froude-scaled model (1:10) was used for simulations. Boundary conditions for monopile and gravity base structures are:

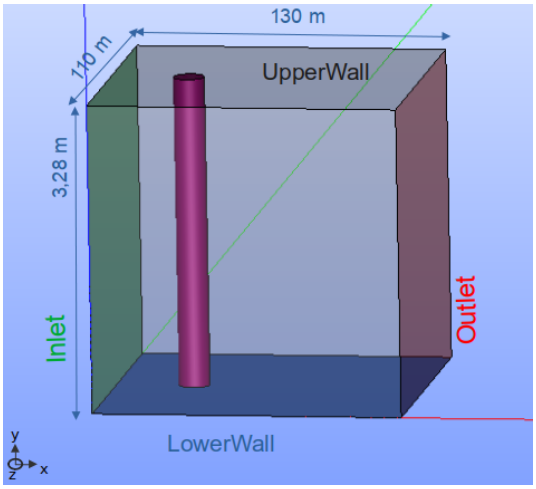

Figure 2: Domain geometry (OWF foundation in pink) with boundaries (Outlet, Inlet, LowerWall).

- $\vec{u} = (0.31\ 0\ 0)$ on $\partial\Omega_1$, uniform flow velocity in x direction,
- $\vec{u} = \vec{0}$ as non-slip condition on $\partial\Omega_2$ and $\partial\Omega_3$ with hypothesis that the seabed is flat,
- $\nabla\vec{u} = 0$ on $\partial\Omega_4$,

where $\partial\Omega_1$, $\partial\Omega_2$, $\partial\Omega_3$, $\partial\Omega_4$ are respectively Inlet, lowerwall, cylinder and outlet as shown in Figure 2. The velocity field values are chosen from realistic values during medium spring tides in Courseulles-sur-Mer [20]. No meteorological forcing was applied. For monopile structure, the cylinder diameter is $d_m = 0.65m$ and for gravity base, we had : top diameter is $d_g = 0.75m$ and base diameter is $D_g = 3.20m$.

2.3 Mesh

A $3D$ base mesh was generated as shown in Figure 3, with 1300 cells in the x-direction, 1100 cells in the y-direction and 16 cells in the z-direction without adding refinement box mesh. Vertical(z) cells were half the size of the horizontal (x-y) cells. A refinement box around the pile in 3 dimensions was chosen in order to capture small processes and strong velocity gradient near the structure.

Table 1: Numerical parameters for OpenFoam on scale 1 : 10 for (A) monopile and (B) gravity base foundation.

	domain size(m)	time step(s)	min cell volume(m^3)	max cell volume(m^3)	refinement box(m)
A	130x110x3.28	0.03	1.6x10^{-5}	0.2x10^{-3}	10x8x3.28
B	130x110x3.28	0.03	5.7x10^{-6}	0.2x10^{-3}	10x8x3.28

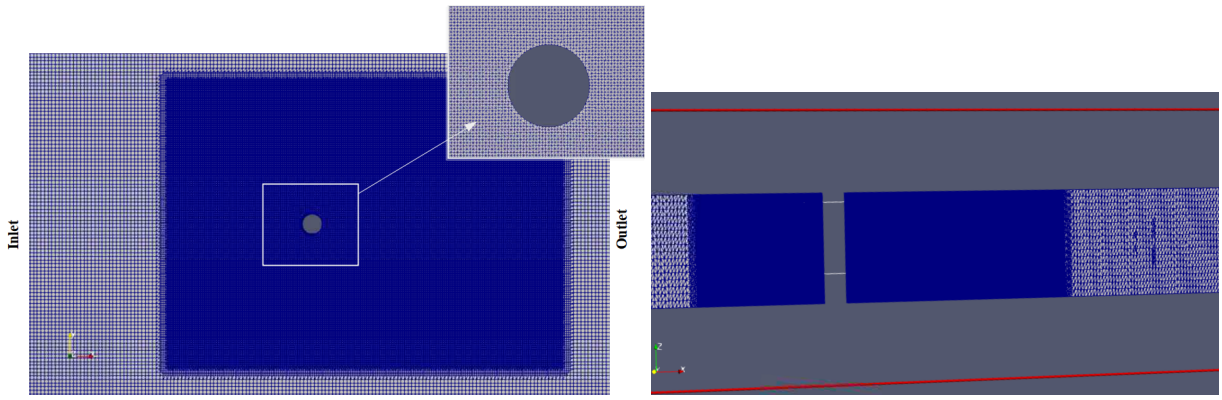

(a) (b)

Figure 3: (a) horizontal view (x-y) of mesh zones with refinement box around the monopile foundation (gray circle),(b) vertical view (x-z) extracted in the center of the pile.

The time step was constrained by the CFL (Courant-Friedrichs-Lewy) condition ([6]) in order to achieve the numerical stability:

$$CFL = U \times \left| \frac{\Delta t}{\Delta x} \right| < 0.5, \tag{6}$$

where U is a free stream velocity, Δt and Δx are the time step and the smallest cell length. To analyze the turbulent wake, the vortex shedding frequency f was used. It was obtained from the non-dimensional Strouhal number St [23]:

$$St = \frac{f \cdot h}{\vec{u}}, \tag{7}$$

where h represented the pile diameter which could be d_m, d_g or D_g. Here, the Strouhal number was found to be quite close to 0.20 relying on the Reynold number for the scale of this study.

2.4 Eulerian-Lagrangian coupling

To pursue the larvae dispersal, biological and hydrodynamical models were coupled. An offline coupling between OpenFoam and Ichthyop was implemented (Figure 4). The Lagrangian transport model for biology, Ichthyop [15], used the flow velocity computed by the hydrodynamic model OpenFoam. Ichthyop released particles and follows their movements [8] using :

$$\frac{\partial \vec{P_p}}{\partial t} = \vec{u_p}, \tag{8}$$

where $\vec{u_p}$ and $\vec{P_p}$ were the particle velocity and position. Larval particles were released at surface and bottom in front of the structure without biological forcing. The initial release time was selected after achieving the current stability time. The particles followed the flow with passive motion which argued by [1].

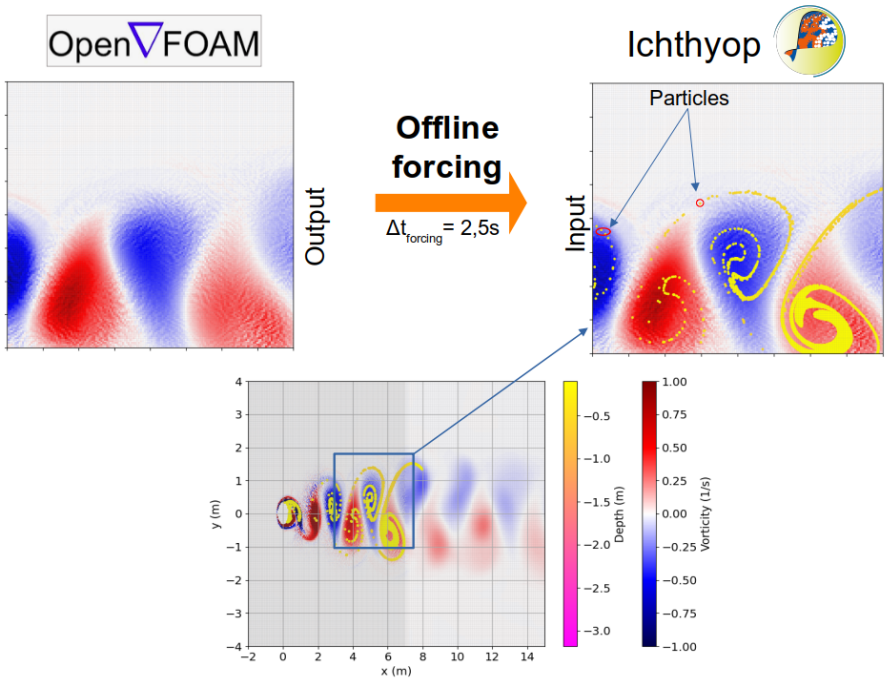

Figure 4: Numerical forcing method (from OpenFOAM to Ichthyop computation).

3 RESULTS

Results were evaluated for two types of foundations, monopile and gravity base structures. The flow around the foundations was examined in 2D and 3D visualisations to match previous works and be in agreement with [12] results.

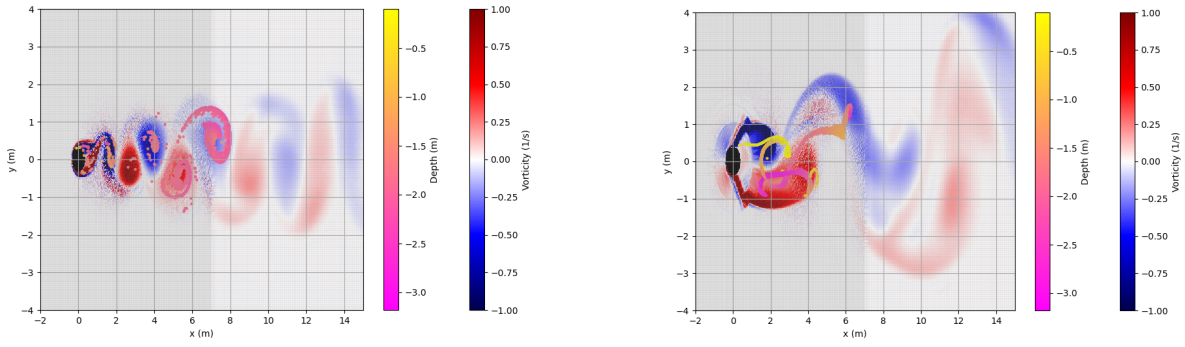

(a) (b)

Figure 5: Horizontal view $(x - y)$ of vorticity magnitude with particles (dots colored by depth position and yellow-pink colorbar) after $30s$ at of release at the surface and in front of the pile. Cases with (a) monopile and (b) gravity base structure.

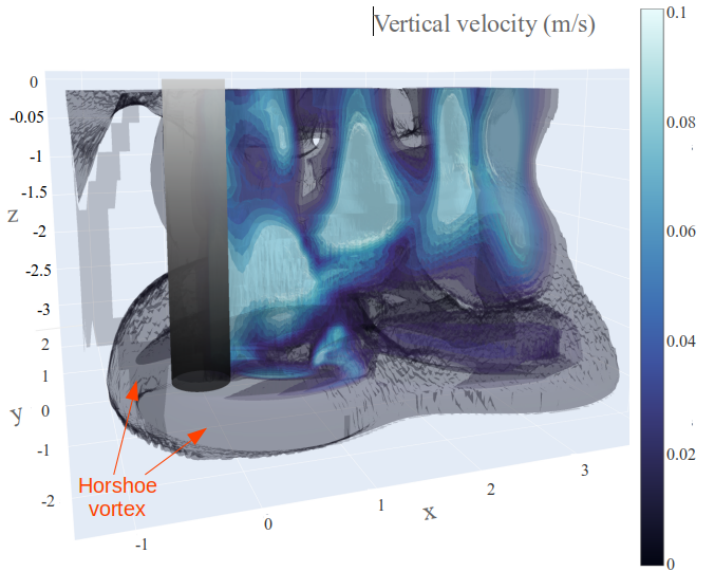

Figure 6: $3D$ visualization (x, y, z=*depth*) of the vertical velocity component U_z. Only positive values are shown, close to the monopile (gray cylinder).

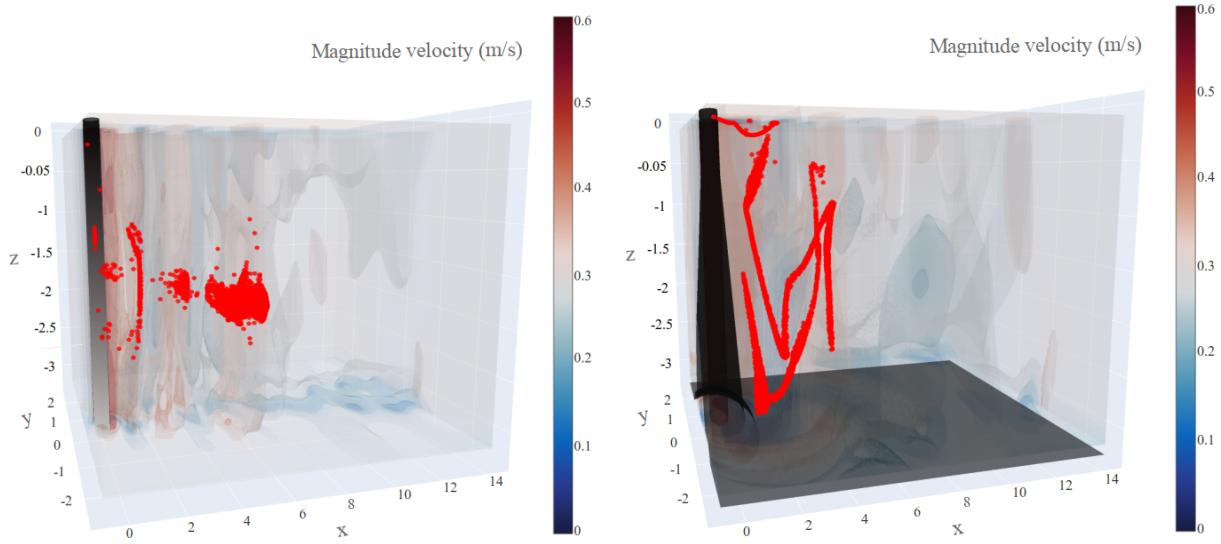

(a) (b)

Figure 7: $3D$ visualization (x, y, z = *depth*) near (a) the monopile and (b) gravity base (black structure) of the velocity magnitude with particles (red dots) released at $2m$ under surface.

When the Reynolds number (Re) is high [10] (over 10^5), the flow is mostly dominated by the Von Kármán street vortices creating a periodic flow (harmonic flow) as shows in Figure 5. This

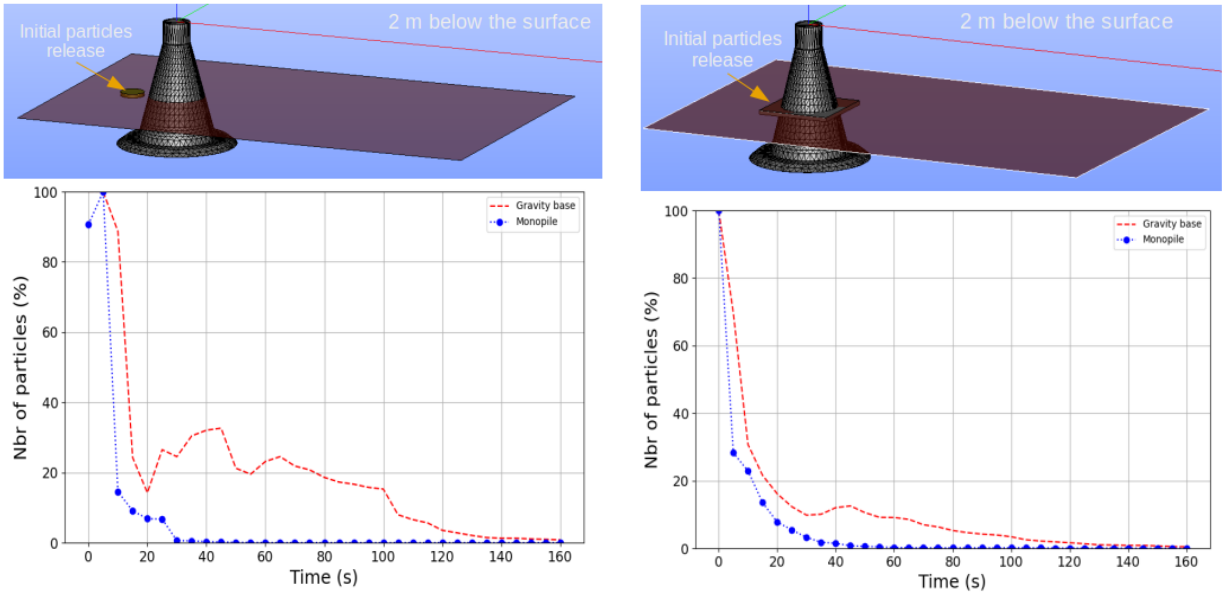

(a) (b)

Figure 8: Sensibility to release type (a) in front of the pile and (b) around the pile in the case of monopile (bleu line) and gravity base (red line) foundations.

vortex shedding may affect the sea bed and generate the horseshoe-vortex downflow around the upstream side of the pile (Figure 6) as described by [18]. Figure 6 shows a 3D view around the structure. Due to an upwelling and downwelling vortex, an important patch of fluid rises up into the surface or rises down from the surface to the bottom, transporting particles from the seabed and bringing them out of the wake and vice versa. The vertical flow of wake vortices (Figure 7) is explained by [18] and can be easily seen by the particles mouvement. The variation of the characteristics of vortices near the foundation impacts especially the vertical larvaes transport. Larval passive vertical velocity ultimately reflects a fluid force on the body motions. For gravity base foundation, there is a faster movement of the particles transport on the vertical probably its the result of the conical large base (Figure 7) comparing to monopile foundation. Also, in order to evaluate the sensitivity to geometry and release type on larval dispersal, the retention time and the number of particles in the retention box around the pile were computed for each case (Figure 8) with different size boxes ($1m$x$1m$x$3.28m$ for monopile foundation and $3.3m$x$3.3m$x$3.28m$ for gravity base foundation) . The intense vertical flow generated by gravity base foundation lead more retention larvae thougth the time but end up without any larvae over $160s$ which is similar to the monopile foundation (Figure 8).

4 CONCLUSIONS

This study shows an evaluation of flow vortex and of the impact of the turbulence in interaction with the structure was shown in 3D numerical model. The larval dispersal is affected by the turbulent wake and stresses present in the 3D numerical simulations. The vertical flow vortices

influence the bottom flow for both types of structures (monopile and gravity base) creating the horshoe vortices. The particle mouvement is forced by Von Kármán vortex above the domain and by the vertical velocity with upward and downward motions. The great grip of the gravity base foundation impact the vertical particles transport and make it vaster than in the case of monopile foundation. Almost similar particles transport with initial release zone around the pile or in front of the pile. All those remarks are valid in the case of the same parameters with uniform velocity, for a flat bottom and similar geometries.

Future work will focus on the impact on larval dispersal for the case of monopile and gravity structures at the regional scale of the two OWFs, by coupling the MARS3D (Model for Applications at Regional Scale) circulation model [14] with Ichthyop using an appropriate parametrization presenting the effects of fondations on the hydro-sedimentary environment [20].

5 ACKNOWLEDGMENTS

This study takes part of a thesis in progress financed by Region Normandy and Agency for the Environment and Energy Management (ADEME). The present work was performed using computing resources of Regional Computer Center and Digital Applications of Normandy (CRIANN) (Normandy, France). The research was made possible at the Continental and Coastal Morphodynamics (M2C) laboratory facilities.

REFERENCES

[1] T. P. Adams, R. G. Miller, D. Aleynik, and M. T. Burrows. Offshore marine renewable energy devices as stepping stones across biogeographical boundaries. *Journal of Applied Ecology*, 51(2):330–338, 2014.

[2] V. Alari and U. Raudsepp. Simulation of wave damping near coast due to offshore wind farms. *Journal of Coastal Research*, 28(1):143–148, 2012.

[3] L. Bergström, L. Kautsky, T. Malm, R. Rosenberg, M. Wahlberg, N. Å. Capetillo, and D. Wilhelmsson. Effects of offshore wind farms on marine wildlife a generalized impact assessment. *Environmental Research Letters*, 9(3):034012, 2014.

[4] E. D. Christensen, M. Johnson, O. R. Sørensen, C. B. Hasager, M. Badger, and S. E. Larsen. Transmission of wave energy through an offshore wind turbine farm. *Coastal engineering*, 82:25–46, 2013.

[5] S. Clark, F. Schroeder, and B. Baschek. *The Influence of Large Offshore Wind Farms on the North Sea and Baltic Sea: A Comprehensive Literature Review.* Helmholtz-Zentrum Geesthacht, Zentrum für Material-und Küstenforschung, 2014.

[6] R. Courant and K. Friedrichs. and H. Lewy. "uber die differenzengleichungen der mathematischen physik". *Math. Ann*, 100:32, 1928.

[7] J. Dannheim, L. Bergström, S. N. Birchenough, R. Brzana, A. R. Boon, J. W. Coolen, J.-C. Dauvin, I. De Mesel, J. Derweduwen, A. B. Gill, et al. Benthic effects of offshore renewables: identification of knowledge gaps and urgently needed research. *ICES Journal of Marine Science*, 77(3):1092–1108, 2020.

[8] F. J. Davidson and B. Deyoung. Modelling advection of cod eggs and larvae on the newfoundland shelf. *Fisheries Oceanography*, 4(1):33–51, 1995.

[9] J. Floeter, J. E. van Beusekom, D. Auch, U. Callies, J. Carpenter, T. Dudeck, S. Eberle, A. Eckhardt, D. Gloe, K. Hänselmann, et al. Pelagic effects of offshore wind farm foundations in the stratified north sea. *Progress in Oceanography*, 156:154–173, 2017.

[10] J. Fredsoe and B. M. Sumer. *Hydrodynamics around cylindrical structures (revised edition)*, volume 26. World Scientific, 2006.

[11] C. J. Greenshields et al. Openfoam user guide. *OpenFOAM Foundation Ltd, version*, 3(1):47, 2015.

[12] N. Kanaris, D. Grigoriadis, and S. Kassinos. Three dimensional flow around a circular cylinder confined in a plane channel. *Physics of Fluids*, 23(6):064106, 2011.

[13] C. Lavanya and N. D. Kumar. Foundation types for land and offshore sustainable wind energy turbine towers. In *E3S Web of Conferences*, volume 184, page 01094. EDP Sciences, 2020.

[14] P. Lazure and F. Dumas. An external–internal mode coupling for a 3d hydrodynamical model for applications at regional scale (mars). *Advances in water resources*, 31(2):233–250, 2008.

[15] C. Lett, P. Verley, C. Mullon, C. Parada, T. Brochier, P. Penven, and B. Blanke. A lagrangian tool for modelling ichthyoplankton dynamics. *Environmental Modelling & Software*, 23(9):1210–1214, 2008.

[16] Y. Liu, Q. Xiao, A. Incecik, C. Peyrard, and D. Wan. Establishing a fully coupled cfd analysis tool for floating offshore wind turbines. *Renewable Energy*, 112:280–301, 2017.

[17] F. R. Menter. Two-equation eddy-viscosity turbulence models for engineering applications. *AIAA journal*, 32(8):1598–1605, 1994.

[18] T. U. Petersen, B. M. Sumer, J. Fredsøe, T. C. Raaijmakers, and J.-J. Schouten. Edge scour at scour protections around piles in the marine environment—laboratory and field investigation. *Coastal Engineering*, 106:42–72, 2015.

[19] J.-P. Pezy and J.-C. Dauvin. Wide coverage but few quantitative data: Coarse sediments in the english channel. *Ecological Indicators*, 121:107010, 2021.

[20] A. Rivier, A.-C. Bennis, G. Pinon, V. Magar, and M. Gross. Parameterization of wind turbine impacts on hydrodynamics and sediment transport. *Ocean Dynamics*, 66(10):1285–1299, 2016.

[21] C. Rogan, J. Miles, D. Simmonds, and G. Iglesias. The turbulent wake of a monopile foundation. *Renewable Energy*, 93:180–187, 2016.

[22] S. Sánchez, J.-S. López-Gutiérrez, V. Negro, and M. D. Esteban. Foundations in offshore wind farms: Evolution, characteristics and range of use. analysis of main dimensional parameters in monopile foundations. *Journal of Marine Science and Engineering*, 7(12):441, 2019.

[23] V. Strouhal. *Über eine besondere Art der Tonerregung*. Stahel, 1878.

[24] J. Van Berkel, H. Burchard, A. Christensen, L. O. Mortensen, O. S. Petersen, and F. Thomsen. The effects of offshore wind farms on hydrodynamics and implications for fishes. *Oceanography*, 33(4):108–117, 2020.